

Lattice dynamics of Cu(110): High-resolution He-scattering study

Peter Zeppenfeld, Klaus Kern, Rudolf David, Klaus Kuhnke, and George Comsa
*Institut für Grenzflächenforschung und Vakuumphysik, Kernforschungsanlage Jülich, Postfach 1913,
5170 Jülich, West Germany*

(Received 23 May 1988)

We report a high-resolution He-scattering study of the clean Cu(110) surface. We have determined the dispersion of the surface phonons along the $\bar{\Gamma}\bar{X}$ and $\bar{\Gamma}\bar{Y}$ symmetry directions. The 19.4-meV resonance near the $\bar{\Gamma}$ point reported in previous electron-energy-loss spectroscopy studies has now also been observed using inelastic He scattering. Along the $\bar{\Gamma}\bar{Y}$ direction we have obtained experimental evidence for phonon scattering from the transverse Cu bulk-band edge. Based on a dynamical model recently proposed by Lehwald *et al.*, a lattice-dynamical slab calculation was performed; taking into account the experimentally determined lattice relaxation of Cu(110) and including surface stress within the topmost layer, good overall agreement is obtained with the experimental results. An examination of the calculated spectral density shows that the transverse bulk-band edge along the $\bar{\Gamma}\bar{Y}$ direction provides a large vibrational amplitude at the surface, which is polarized in the sagittal plane and thus can be observed experimentally. The crossover between the bulk-band edge and a surface resonance of the same symmetry is avoided, and a hybridization of these modes is observed at a wave vector $Q = 0.70Q_{BZ}(\bar{Y})$. Beyond this point the surface vibrational amplitude of the bulk-band edge strongly decreases, while the lower branch, which has then become a true surface mode, still has a large vibrational amplitude in the sagittal plane.

I. INTRODUCTION

The dynamical properties of crystal surfaces are of fundamental importance for a wide range of processes of interest in surface chemistry and surface physics, such as adsorption and desorption of gases, energy accommodation in gas-surface reactions, phase transitions, and the reconstruction of surfaces.¹ The basic information on the dynamical properties of surfaces is obtained from the investigation of the dispersion and polarization vectors of surface phonons. The first detailed theoretical analysis of the surface-phonon dispersion on different faces of clean and adsorbate-covered fcc metals was carried out by Allen, Alldredge, and de Wette in 1971.² At that time there were no experimental data on the dispersion of surface phonons, and therefore a possible modification of the bulk force field in the surface region could only be speculated. It took ten years until the first surface-phonon dispersion was measured on a LiF(001) surface using inelastic He-atom scattering.³ During the last five years, however, a considerable number of experimental studies on a wide range of clean and adsorbate-covered surfaces has been reported.⁴ Two powerful techniques have been developed to achieve the sensitivity and resolution necessary for these kind of experiments: high-resolution electron-energy-loss spectroscopy (HREELS) (Ref. 5) and high-resolution He-atom scattering.⁶

The investigation of the surface vibrations of the (111) and (100) faces of several fcc metals has shown that in general the surface-phonon dispersion is quite different from what is expected for a bulklike force field at the surface.² For example the appearance of a new surface resonance and the softening of the Rayleigh wave frequency at the zone boundary was observed on the (111) faces of

Cu, Ag, Au, and Pt.^{7,8} Both features could be explained by a considerable reduction of the nearest-neighbor force constant between the atoms within the first layer, as a consequence of the redistribution of the electronic charge near the surface [nevertheless, in the case of Cu(111), the actual magnitude of this reduction is still controversial⁹]. In contrast, the (100) surfaces of Cu and Ni exhibit an increased Rayleigh wave frequency, which can be explained by a stiffening of the force constant acting between the first and second layer.¹⁰ On the other hand, a tensile stress within the topmost layer can equally well describe the observed frequency.¹¹

From a lattice dynamical point of view, among the low-indexed faces of the fcc metals, the (110) surface is of particular interest: In the bulk-force-field model² the (110) face shows a large number of surface phonons and resonances. On the other hand, on the open (110) surface, the change of the bulk force field is expected to be very important. Indeed, a large lattice relaxation has been observed,¹² and there is a strong tendency of the (110) surfaces to reconstruct.¹³ Furthermore, the surface modes of the (110) face at the high symmetry points are strictly unidirectionally polarized parallel or perpendicular to the surface. This makes a lattice dynamical analysis very effective and unambiguous, since the change of a particular force constant at the surface only influences specific modes with the appropriate symmetry, as shown by Lehwald *et al.*¹⁴ In spite of these appealing features, except for one early He-scattering experiment on Cu(110),¹⁵ the (110) faces of fcc metals have attracted attention only very recently: in 1987 phonon-dispersion measurements were reported on the (110) faces of Al,¹⁶ Ag,¹⁷ Pd,¹⁸ and Ni.¹⁴ Several interesting, unpredicted features have been observed on these surfaces, such as an

acoustical surface resonance along the $\bar{\Gamma}\bar{X}$ direction. Moreover, there has been some controversy on the actual number and on the interpretation of the acoustical modes along the other high-symmetry direction $\bar{\Gamma}\bar{Y}$.

The main result of this paper is that our scattering data on one hand point out a number of surface vibrational modes in accordance to the results on related (110) surfaces; on the other hand, we are able to reconcile the existing controversial arguments concerning the phonon dispersion along $\bar{\Gamma}\bar{Y}$. We find direct experimental evidence of phonon scattering from the transverse bulk-band edge as one would expect from an intrinsic branch. A comparison with our lattice dynamical calculation supports this result and additionally reveals a surprising interaction of this bulk-band edge with a second, real, surface resonance.

The paper is organized as follows. In the next section, we outline the main features of the He-scattering apparatus; we discuss the measured phonon-scattering data and the experimental surface-phonon dispersion of the clean Cu(110) surface. In Sec. III a simple lattice dynamical model is presented and used to fit the experimental data. Finally, in Sec. IV the spectral densities along the $\bar{\Gamma}\bar{Y}$ direction, calculated from the best fit are analyzed, and the interpretation of our scattering data is given. This result is compared to the results obtained on related (110) metal surfaces.

II. EXPERIMENTAL RESULTS

The measurements were performed with the high-resolution He-scattering apparatus described in detail elsewhere.¹⁹ Here we will only outline those features which are of particular relevance for the present study.

A He nozzle-beam generator supplies a high-intensity primary He beam with an energy spread of $\Delta E_i/E_i = 1.4\%$ (FWHM). By cooling and heating the nozzle in a temperature range from 30 to 800 K, the He-beam energy E_i is continuously adjustable between 6.5 and 170 meV. The He-beam generator and the detector being immobile, the total scattering angle is fixed: $\theta_i + \theta_f = 90^\circ$. The scattering conditions are varied by rotating the crystal, thereby changing θ_i and θ_f relative to each other. The angular divergence of the incident beam and the angle subtended by the detector are both 0.2° . Pseudorandom chopping is used for time-of-flight analysis of the scattered He atoms.^{19,20} The energy distribution of the scattered beam is then plotted, and from the characteristic single-phonon-loss and/or -gain peaks the information on the surface-phonon dispersion is obtained. Under typical scattering conditions ($E_i = 18.3$ meV and the width of a single time-of-flight channel $\tau = 2.5 \mu\text{s}$) a total energy resolution of $\Delta E \sim 0.36$ meV (FWHM) is obtained. Conservation of parallel momentum and energy can be used to relate the observed phonon energy $\hbar\omega$ and the corresponding parallel momentum Q transferred from the He beam. In the special case of a fixed geometry ($\theta_i + \theta_f = 90^\circ$) this relation reads

$$\hbar\omega = E_i \left[\left(\frac{\sin\theta_i + Q/k_i}{\cos\theta_i} \right)^2 - 1 \right]. \quad (1)$$

This expression is frequently referred to as the *scan curve*. It implies that at a particular angle of incidence θ_i only the phonons having Q and $\hbar\omega$ values related through Eq. (1) can be observed experimentally.

The base pressure in the scattering chamber is in the low 10^{-11} mbar range. The Cu(110) surface was cleaned by successive cycles of sputtering and heating. The quality of the surface was controlled by AES and LEED and finally by monitoring the intensity of the diffracted and the diffuse elastic-scattered He beam.

In Fig. 1 we recall the unit cell of the (110) surface of a fcc crystal and the corresponding first Brillouin zone in reciprocal space. Also indicated are the high-symmetry points $\bar{\Gamma}$, \bar{X} , \bar{Y} , and \bar{S} following the commonly used notation.

A series of measured time-of-flight spectra of the clean Cu(110) surface with the wave-vector transfer Q along the $\bar{\Gamma}\bar{X}$ symmetry direction is shown in Fig. 2. Note that spectra 2(b) and 2(c) were taken using the same incident He-beam energy $E_i = 39.6$ meV, but for different angle of incidence θ_i . Spectrum 2(a) was obtained using a primary energy $E_i = 18.3$ meV. For convenience the time of flight has been converted to an energy scale, zero energy corresponding to the elastically scattered beam. The assignment of the individual phonon modes will be explained in detail in the following section; here the labels are only used to designate different modes. Spectrum 2(a) shows a strong energy loss at -1.7 meV (S_1) which is attributed to the Rayleigh wave. The weak feature at -7.6 meV also originates from the Rayleigh wave: Under the particular scattering conditions ($E_i = 18.3$ meV, $\theta_i = 42.5^\circ$) Eq. (1) is fulfilled twice for the S_1 mode, for $Q = 0.16 \text{ \AA}^{-1}$ ($\hbar\omega = -1.7$ meV) and $Q = -0.67 \text{ \AA}^{-1}$ ($\hbar\omega = -7.63$ meV). In spectrum 2(b) a second mode (MS_0), later identified as an acoustical surface resonance, is observed. Finally spectrum 2(c) again shows phonon losses attributed to the S_1 and MS_0 mode, respectively, but in addition a sharp loss at -19.4 meV is clearly apparent. From Eq. (1) a corresponding wave vector $Q = 0.09 \text{ \AA}^{-1}$ is evaluated, indicating that this surface phonon is located near the $\bar{\Gamma}$ point. This result is to be compared to the observation of a dipole active resonance on Cu(110) and Ni(110), measured with EELS:²¹⁻²³ for Cu(110) an energy of $\hbar\omega \approx 20$ meV was found at the $\bar{\Gamma}$ point. We may therefore identify the loss labeled MS_7 in Fig. 2(c) with that same resonance. Since we were able to

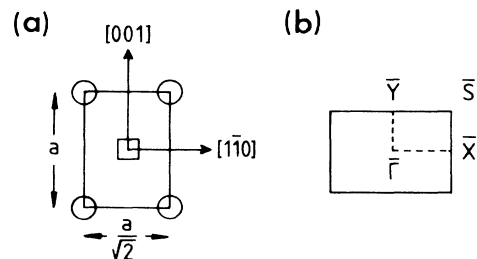


FIG. 1. Surface unit cell of the fcc (110) face (a) and first Brillouin zone of the corresponding reciprocal lattice (b), including the notation of the high-symmetry points. The circles and the square (a) indicate first- and second-layer atoms, respectively.

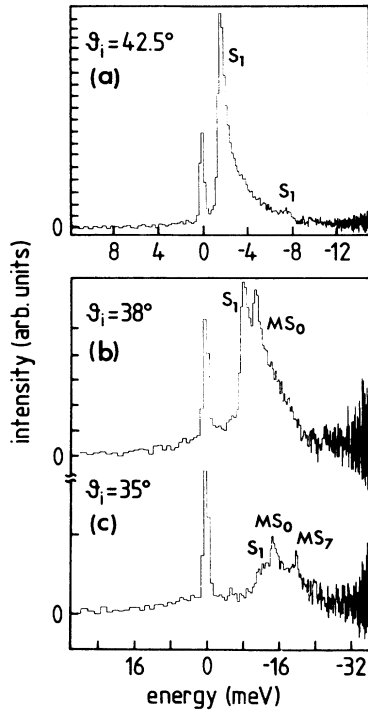


FIG. 2. He time-of-flight spectra taken along the $\bar{\Gamma}\bar{X}$ direction converted to an energy scale (negative values indicate phonon creation, positive values phonon annihilation). The primary He-beam energy was 18.3 meV (a) and 39.6 meV (b) and (c), respectively. The increase of the noise at higher phonon-loss energies is a feature of the conversion from the time of flight to the energy scale. The phonon peak labels are explained in Secs. III and IV.

measure this “dipole-active” resonance with He scattering, it must have a significant vibrational amplitude within the topmost surface layer, polarized in the z direction (normal to the surface). Note from Fig. 2 that the intensities of the S_1 and MS_0 phonons strongly decrease with decreasing θ_i , i.e., with increasing wave vector Q . In Fig. 3 the experimental phonon-dispersion data along the $\bar{\Gamma}\bar{X}$ direction obtained from a number of spectra like those in Fig. 2 are plotted. The intensity decrease of the S_1 and MS_0 phonons is reflected in the absence of data points for these modes close to the zone boundary \bar{X} .

In analogy with the measurements along the $\bar{\Gamma}\bar{X}$ direction presented above, the phonon dispersion of Cu(110) was also measured along $\bar{\Gamma}\bar{Y}$. Figure 4 shows three spectra with the Cu(110) surface oriented along the $\bar{\Gamma}\bar{Y}$ direction, taken with a primary He-beam energy $E_i = 18.3$ meV. Spectrum 4(a) shows two distinct loss features at -4.2 and -8.1 meV, respectively. Although the main peak at -4.2 meV is labeled E , indicating scattering from the transverse bulk-band edge (as will be explained in the following sections), there is a large contribution of the Rayleigh wave S_1 , and a tail extending to the high-energy-loss side due to a resonance mode (S_3) is observed. The second loss feature at -8.1 meV again originates from scattering by the S_3 mode, however, at a different wave vector than for its contribution to the tail

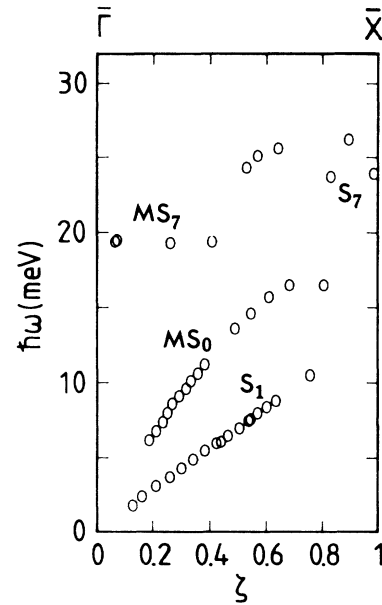


FIG. 3. Experimental data points along the $\bar{\Gamma}\bar{X}$ direction, plotted in a reduced zone scheme. ζ denotes the reduced wave vector defined through $\zeta = Q/Q_{BZ}(\bar{X})$, with $Q_{BZ}(\bar{X}) = 1.23 \text{ \AA}^{-1}$.

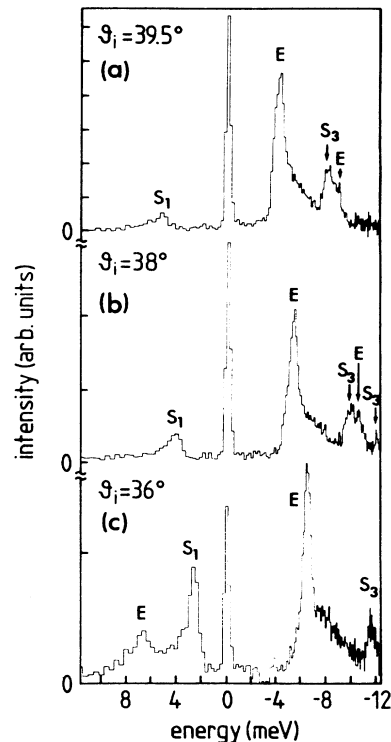


FIG. 4. He-scattering spectra as in Fig. 2, but taken along the $\bar{\Gamma}\bar{Y}$ direction. The primary He-beam energy was 18.3 meV in all three spectra.

of the first peak.

With some imagination a shoulder (E) at about -9 meV may be distinguished. Note that in addition a small phonon-annihilation peak around 5 meV is observed, which is attributed to the Rayleigh wave (S_1). Spectrum 4(b) is similar to 4(a), however, the "shoulder" of the second loss peak is now clearly separated as a third mode (E). Furthermore, at -12.0 meV an extra loss peak has appeared, which again is due to S_3 (at a wave vector close to the zone boundary). Note that this peak is much narrower and exhibits no shoulder. We will discuss this behavior in more detail in Secs. III and IV. Finally spectrum 4(c) shows a broadened loss peak at -11.8 meV ($Q = -0.61 \text{ \AA}^{-1}$), which is labeled S_3 , although probably an admixture of E is present. The gain peak due to Rayleigh wave (S_1) at 2.4 meV has now become very intense and in addition a second gain feature at 6.6 meV (E) is observed. It should be pointed out that the corresponding Q values (1.6 and 2.1 \AA^{-1} for the 2.4 - and the 6.6 -meV gain, respectively) are quite large, extending into the higher Brillouin zones [$Q_{\text{BZ}}(\bar{Y}) = 0.87 \text{ \AA}^{-1}$]. Figure 5 summarizes the experimental results obtained for the $\bar{\Gamma}\bar{Y}$ direction. As for the $\bar{\Gamma}\bar{X}$ direction, a series of high-energy phonons (using an incident beam energy $E_i = 39.6$ meV) were observed.

While Fig. 5 shows the data points backfolded into the first Brillouin zone [$0 \leq Q \leq Q(\bar{Y})$], it is instructive to plot the same set of data points with the corresponding original wave vectors. This is shown in Fig. 6. Also plotted are three scan curves corresponding to the scattering

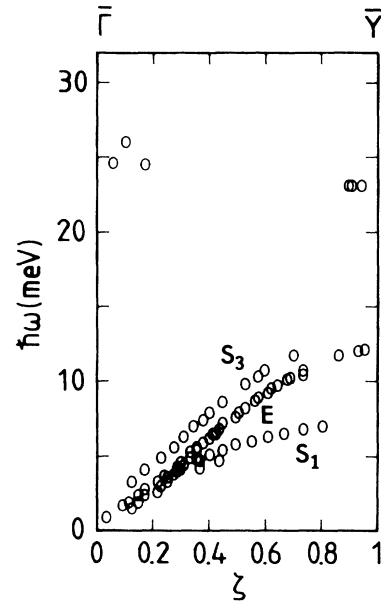


FIG. 5. Same as Fig. 3, but along the $\bar{\Gamma}\bar{Y}$ direction. $\zeta = Q/Q_{\text{BZ}}(\bar{Y})$ with $Q_{\text{BZ}}(\bar{Y}) = 0.87 \text{ \AA}^{-1}$.

conditions of the spectra in Fig. 4. It is now obvious how changing the scattering conditions (i.e., the scan curve) can produce the different shapes of the S_3 and E loss features evidenced in Fig. 4. As already noted above and further evidenced in Fig. 6, scattering from the Rayleigh wave is most effective at large parallel momentum

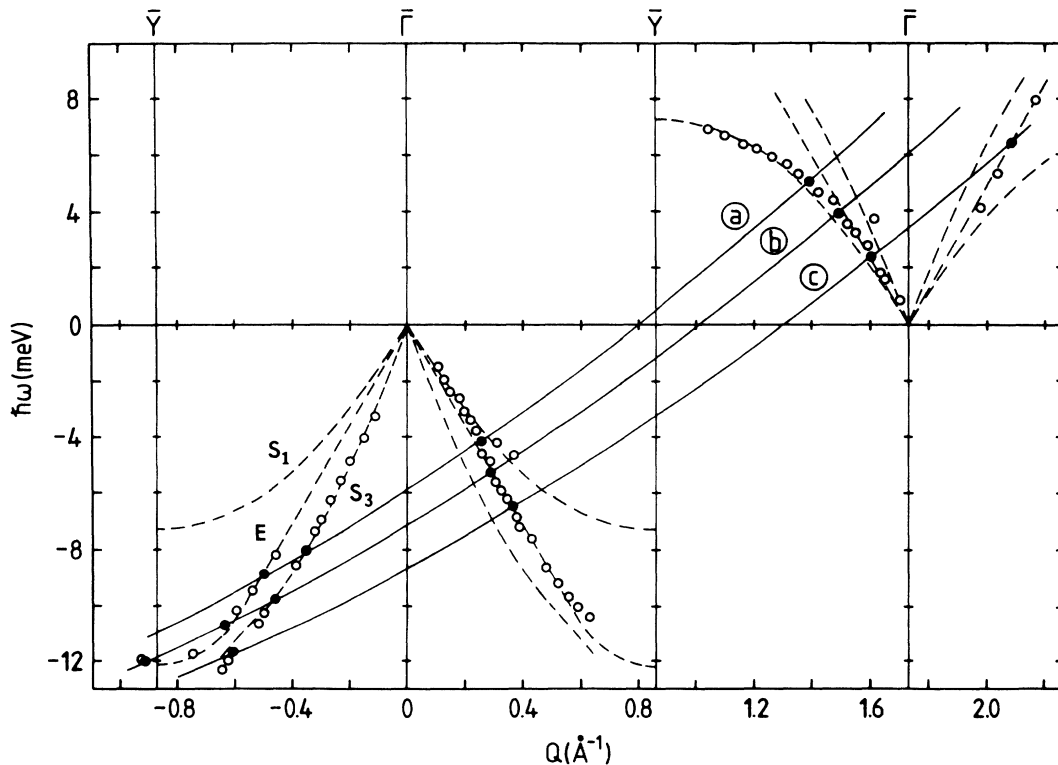


FIG. 6. Same data set as in Fig. 5, but plotted in an *extended* zone scheme, with the actually measured Q values. The solid lines (a), (b), and (c) are the scan curves [Eq. (1)] corresponding to the scattering conditions in Fig. 4 ($E_i = 18.3$ meV and $\theta_i = 39.5^\circ$, 38° , and 36° , respectively). The dashed lines through the data points are calculated from a dynamical model fitted to the scattering data (see Sec. III).

transfer Q . As we will see in the following sections, the Rayleigh wave along $\bar{\Gamma}\bar{Y}$ is mainly longitudinally polarized (i.e., polarized in the [001] direction). This may be rationalized by the fact that there are indeed no nearest neighbors in the surface plane along the [001] direction and therefore the lowest-lying vibrational surface mode—the Rayleigh wave—along $\bar{\Gamma}\bar{Y}$ is expected to have a large amplitude in the [001] direction and thus will be strongly longitudinally polarized. This longitudinal polarization might explain the enhanced scattering from the Rayleigh wave at high parallel momentum transfer along the [001] direction. Indeed, the scattering cross section for inelastic He scattering sensitively depends on the product $Q \cdot \mathbf{e}_l$, where \mathbf{e}_l denotes the polarization vector of the phonon in the topmost surface layer.

III. LATTICE DYNAMICAL CALCULATIONS

In the previous section we reported the experimentally determined surface-phonon dispersion curves of Cu(110) along the $\bar{\Gamma}\bar{X}$ and $\bar{\Gamma}\bar{Y}$ high-symmetry directions. Now the question arises how these particular modes can be explained theoretically: what influence does the surface modified force field have on the phonon dispersion and how can it be modeled?

Since the only *ab initio* calculations carried out so far are done for Al(110),^{24,25} we have to content ourselves with more phenomenological models, by fitting individual force constants to the experimental dispersion curves. To our knowledge the only such calculation for Cu(110) was carried out by Black *et al.*²⁶ They fitted the only experimental data available at that time (Mason, McGreer, and Williams¹⁵). These data gave valuable information on the phonon dispersion along the $\bar{\Gamma}\bar{Y}$ direction; for instance three different acoustical phonon branches could be observed. However, no optical resonances were reported and the $\bar{\Gamma}\bar{X}$ direction was not investigated at all. A comparison of the data (Fig. 2 of this work and Figs. 5 and 7 of Ref. 15) shows that the present study reveals more details and provides additional information on the dispersion at the zone boundary—which is of particular importance when fitting force constants in a lattice dynamical model. We therefore believe that a lattice dynamical calculation on the basis of the present data for Cu(110) is worthwhile.

In order to obtain an unambiguous interpretation of the data, a simple lattice dynamical model is required, with a minimum number of fitting parameters. The simplest model certainly is the nearest-neighbor central-force model, where only one parameter—the nearest-neighbor force constant ϕ'' —is needed. It should be pointed out here, that this model can already reproduce the bulk phonon-dispersion curves of Cu, determined by means of inelastic neutron scattering,²⁷ with an accuracy of a few percent.²⁸ The best fit to the Cu-bulk data yields $\phi'' = 2.7 \times 10^4$ dyn/cm. We will use this single force constant to describe the dynamical properties of the inner layers of the Cu slab crystal. Changes to this value and additional force constants are only introduced in the very near surface region (mainly in the topmost layer).

In Fig. 7 the phonon-dispersion curves of a Cu(110)

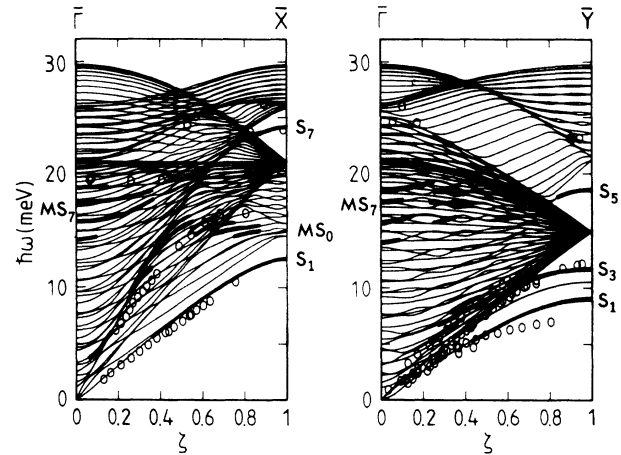


FIG. 7. Phonon-dispersion curves of a 30-layer-thick (110) slab crystal along $\bar{\Gamma}\bar{X}$ and $\bar{\Gamma}\bar{Y}$. A simple bulklike nearest-neighbor central-force model was used, with the bulk force constant $\phi'' = 2.7 \times 10^4$ dyn/cm. Thick solid lines indicate phonon modes for which the contribution of the vibration along the longitudinal or the z direction of the topmost layer to the total squared vibrational amplitude (summed over all layers and all three direction x , y , and z) is $\geq 10\%$. The open circles indicate the experimental data (Figs. 3 and 5).

slab crystal are shown, calculated for a 30-layer-thick slab using only the bulk force constant $\phi'' = 2.7 \times 10^4$ dyn/cm. Experimentally observable surface phonons, i.e., phonon branches which have a significant amplitude in the topmost layer polarized in the sagittal plane are marked by thick solid lines. In order to facilitate the comparison between experiment and theory, the experimental data points (Figs. 3 and 5) are also plotted. It is readily seen from Fig. 7 that the experimental data along the $\bar{\Gamma}\bar{X}$ direction are fairly well reproduced by the simple bulk-force-field model. A similar result was obtained in the case of Ag(110).¹⁷ The dispersion of the MS_0 and MS_7 mode is explained by an avoided crossing, predicted to occur on the (110) faces of fcc metals by Persson, Strocio, and Ho²² and observed experimentally on Ag(110) by Bracco *et al.*¹⁷ This avoided crossing also explains the interchange of polarization between the MS_0 and the MS_7 resonances: being mainly longitudinally polarized at small wave vectors, the MS_7 resonance takes over the z polarization of the MS_0 resonance at intermediate wave vectors. Finally, the vibrational amplitude of the MS_0 resonance decreases and is again longitudinally polarized at the \bar{X} point. Note that the phonons near the \bar{X} point (at 24–26 meV) correspond to the gap mode (S_7) and an upper bulk-band edge. The most remarkable feature, however, is the dispersion of the second mode along $\bar{\Gamma}\bar{Y}$ labeled E in Fig. 5. In the reduced-wave-vector range $0.4 \leq \zeta \equiv Q/Q(\bar{Y}) \leq 0.7$ the experimental data points coincide with the lowest (transverse) bulk-band edge. Indeed, the spectral density indicates that in this wave-vector range there is a significant sagittal vibrational amplitude at the bulk edge. Besides S_1 and E , a third mode—the surface resonance S_3 —can also be dis-

tinguished. It bends towards the bulk edge at $\zeta=0.7$, however, the crossing of both modes is avoided: the edge mode peels off the bulk edge becoming a true surface mode at higher ζ values. This interesting behavior will be discussed in more detail in the following section. For historical reasons,² and because it originates from the avoided crossing, the persisting surface mode for $\zeta > 0.7$ is still labeled S_3 [see Figs. 4(c) and 6]. Note that the surface mode located between S_1 and S_3 is shear horizontal (polarized perpendicular to the sagittal plane) and therefore not detectable in experiment. The gap mode (S_5) at ~ 18 meV near $\bar{\Gamma}$ is longitudinally polarized. Such modes are in general less efficiently detected, which might be the reason why, to our knowledge, the S_5 mode has never been measured so far on any (110) fcc surface. It is surprising that the surface resonance near the $\bar{\Gamma}$ point is not also observed along the $\bar{\Gamma}\bar{Y}$ direction; we have no explanation so far.

In spite of the good qualitative agreement along the $\bar{\Gamma}\bar{X}$ direction, a more detailed analysis of the spectral density of states at the $\bar{\Gamma}$ point indicates that the MS_7 resonance is quite broad and centered around $\hbar\omega \approx 18$ meV, which is too low compared to the experimental result ($\hbar\omega = 19.4$ meV). The largest discrepancy, however, is observed along the $\bar{\Gamma}\bar{Y}$ direction; in particular, the dispersion of the lowest-lying mode (the Rayleigh wave) is not well reproduced. Remember, that the calculated dispersion curves in Fig. 7 were obtained with the *bulk* force constant only.

In the following we will outline how the qualitative agreement evidenced in Fig. 7 can be made quantitative by slightly modifying the bulk force field in the surface region. Physically these changes originate from the "cutting" of bonds at the surface, leading to a charge redistribution in the surface region, which of course alters the local force field. The most striking and well-known consequences are the relaxation and/or reconstruction of surfaces. In the case of the (110) metal surfaces a substantial oscillatory relaxation is observed, leading to a contraction of the spacing between the first and second layer and an expansion between the second and third layer. In a recent medium energy ion scattering (MEIS) study²⁹ the lattice relaxation for Cu(110) was found to be $\Delta d_{12} = -7.5\%$ and $\Delta d_{23} = +2.5\%$. Values scattering slightly around these numbers have been reported in earlier LEED and MEIS studies (see, e.g., quotations in Ref. 29). This relaxation changes the interlayer force field at the surface; even in a simple nearest-neighbor model a nonvanishing Δd_{12} and Δd_{23} will influence the force constants between the first four layers. In order to keep the number of free parameters as small as possible and the physical interpretation straightforward, a simple model connecting the lattice relaxation with the force constant changes is requested. Such a model was recently proposed by Lehwald *et al.*¹⁴ They have scaled the radial, interlayer force constants to the experimentally determined relaxation in the spirit of Badger's rule (originally applied to the vibration in molecules³⁰). In this way they could well describe the features which are known to be most sensitive to the interlayer force constants; in particular the frequency and the linewidth of the MS_7 reso-

nance at $\bar{\Gamma}$. Following¹⁴ the force constant between layers i and j is related to the interlayer spacing r_{ij} through

$$\frac{\phi''_{ij}}{\phi''_b} = \left(\frac{r_b}{r_{ij}} \right)^\alpha, \quad (2)$$

where the subscript b denotes bulk values. By fitting the dipole resonance, Lehwald *et al.* obtained $\alpha=8$ which is in agreement with the values obtained for molecules. In a similar way we monitored the shape of the MS_7 resonance at the $\bar{\Gamma}$ point as a function of α . Note, however, that due to the different scattering mechanisms of EELS and He scattering here the vibrational amplitude of the topmost layer perpendicular to the surface is relevant and not the relative displacement of the first and second layers. We find that with increasing α ($0 \leq \alpha \leq 12$) the spectral width of the resonance, as deduced from the spectral density, decreases and that its frequency is significantly increased (Fig. 8). The experimental value $\hbar\omega = 19.4$ meV is best reproduced for $\alpha \approx 8$ which is in excellent agreement with Ref. 14. This agreement is an additional support of the applicability of a scaling rule to the dynamical modeling of lattice relaxation. Indeed, direct experimental evidence of Badger's rule has recently been obtained for Cu(110). Baddorf *et al.*³¹ have studied the removal of the lattice relaxation of the Cu(110) surface at 100 K upon hydrogen adsorption.³² The authors observed that both lattice spacings d_{12} and d_{23} return to the bulk spacing with increasing hydrogen coverage. With specular EELS the frequency of the $\bar{\Gamma}$ resonance was monitored and could be related to the lattice spacing through $\hbar\omega \sim d_{12}^{1.8 \pm 0.7}$. The simple nearest-neighbor central-force model can be used to link the surface constants with the interlayer spacing of Cu(110). Baddorf and Plummer obtained

$$\frac{\phi''_{12}}{\phi''_b} = \left(\frac{d_b}{d_{12}} \right)^{7.3 \pm 3}$$

which again is in very good agreement with our result.

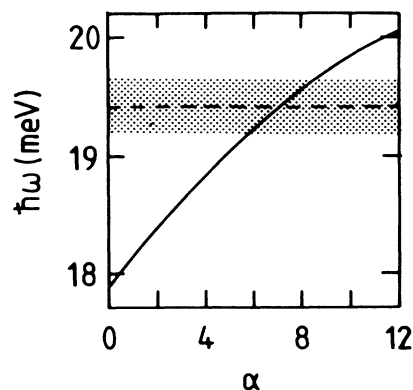


FIG. 8. Vibrational energy of the MS_7 resonance at the $\bar{\Gamma}$ point as a function of α [Eq. (2)], as obtained from the spectral density of states calculated with the force constants ϕ''_{12} , ϕ''_{13} , ϕ''_{23} , and ϕ''_{24} modified according to Eq. (2). The experimentally determined lattice relaxation Δd_{12} and Δd_{23} was used to calculate r_{ij} in Eq. (2). The measured energy $\hbar\omega_7 = 19.4 \pm 0.24$ meV, also shown in the figure, is best reproduced for $\alpha \approx 8$.

Thus taking the best-fit value $\alpha=8$, Badger's rule yields the modified interlayer nearest-neighbor force constants listed in Table I, taking into account the changes to the bulk force field due to the lattice relaxation ($\Delta d_{12} = -7.5\%$ and $\Delta d_{23} = +2.5\%$) of the Cu(110) surface. The MS_7 resonance is now well reproduced, however, there still remain significant deviations from other surface modes (in particular from the Rayleigh wave along $\bar{\Gamma}\bar{Y}$). In their study of the Ni(110) surface, Lehwald *et al.* have developed a detailed procedure, based on symmetry arguments, showing how the different surface modes can be successively fitted to the experimental curves: By changing the intralayer force constant within the first layer ϕ''_1 , and allowing for an (anisotropic) surface stress in the topmost layer ($\sqrt{2}\phi''_{11x}/a$ and ϕ''_{11y}/a , denoting the tangential force constants along $[110]$ and $[001]$, respectively), and finally introducing a second neighbor force constant $\phi''_{11}(2)$, which models the coupling between the close-packed atomic rows in the topmost layer, the experimental data on Ni(110) could be unambiguously fitted, and the role of surface stress was clearly demonstrated.

Following this procedure, we determined the corresponding force constants for Cu(110) which give the best fit to our experimental data. The resulting force constants are listed in Table II; Fig. 9 shows the quantitative overall agreement of the calculated dispersion curves (using the force constants of Tables I and II) with experiment. As an example, the fit of the Rayleigh wave along $\bar{\Gamma}\bar{Y}$ is briefly illustrated: Due to the longitudinal polarization (B_1 symmetry character) of the Rayleigh wave (S_1) and the transverse polarization of the S_3 mode at the \bar{Y} point, ϕ''_{11y} only affects the S_3 mode and $\phi''_{11}(2)$, coupling second neighbors in the $[001]$ direction, will only change the frequency of the S_1 mode (both force constants clearly have no influence on the phonon dispersion along $\bar{\Gamma}\bar{X}$). Because of its A_1 symmetry, character at \bar{X} , the Rayleigh wave along $\bar{\Gamma}\bar{X}$ is affected by ϕ''_{11x} . Therefore the value $\sqrt{2}\phi''_{11x}/a = -0.10\phi''_b$ indicates that a compressive stress $\tau_{[1\bar{1}0]} = -1.9 \times 10^3$ dyn/cm, trying to expand the surface along the $[1\bar{1}0]$ direction, is required to properly describe the Rayleigh wave along $\bar{\Gamma}\bar{X}$. $\phi''_{11}(2) = -0.12\phi''_b$ is necessary to soften the Rayleigh wave along $\bar{\Gamma}\bar{Y}$.

Comparing the values of Table II with those of Ref. 14, there is a difference in sign and relative magnitude of the surface stress. While Lehwald *et al.* report a large stress of 4.2×10^3 dyn/cm along the $[001]$ direction of the Ni(110) surface, the corresponding value for Cu(110) is practically zero. Furthermore, along the $[1\bar{1}0]$ direction the stress is tensile for Ni(110) but compressive for Cu(110). The presence of surface stress might indicate

TABLE I. Interlayer force constants resulting from the scaling according to Eq. (2) with $\alpha=8$ and a relaxation of $\Delta d_{12} = -7.5\%$ and $\Delta d_{23} = -2.5\%$.

ϕ''_{12}/ϕ''_b	ϕ''_{13}/ϕ''_b	ϕ''_{23}/ϕ''_b	ϕ''_{24}/ϕ''_b
1.158	1.225	0.951	0.905

TABLE II. Best-fit intralayer force constants in the topmost surface layer.

ϕ''_{11}/ϕ''_b	$\left[\frac{\sqrt{2}\phi''_{11x}}{a}\right]/\phi''_b$	$\left[\frac{\phi''_{11y}}{a}\right]/\phi''_b$	$\phi''_{11}(2)/\phi''_b$
0.90	-0.10	0.01	-0.12

the tendency of the surface to reconstruct. More precisely, the tensile stress on Ni(110) along $[1\bar{1}0]$ would be in agreement with the pairing-row-type (1×2) reconstruction of H/Ni(110),³³ while a compressive stress along $[001]$ on Cu(110) supports a missing-row (2×1) reconstruction of O/Cu(110).³⁴ However, these arguments remain highly speculative, because the surface force field is obviously changed upon hydrogen or oxygen adsorption.

IV. DISCUSSION

In this section we will draw our attention to a more detailed investigation of the three acoustical modes along the $\bar{\Gamma}\bar{Y}$ direction (i.e., the S_1 , E , and the S_3 mode). Finally we will compare our results to those obtained on related (110) metal surfaces.

Figure 10 shows the spectral density of states calculated for a 60-layer-slab crystal, using the best-fit parameters for Cu(110) (Tables I and II), at three different values of the reduced wave vector ζ along the $\bar{\Gamma}\bar{Y}$ direction. Only modes polarized in the sagittal plane (longitudinally, dashed lines, and z polarized modes, solid lines) are displayed. Three modes are clearly distinguished: The lowest-lying mode corresponding to the Rayleigh wave (S_1)—note its mainly longitudinal polarization—and a doublet around 10 meV, which is strongly z polarized. Here we want to focus on the characteristic dispersion of this doublet. Comparing Figs. 9 and 10, the mode at 9.2 meV in Fig. 10(a) ($\zeta=0.6$) is assigned to the transverse

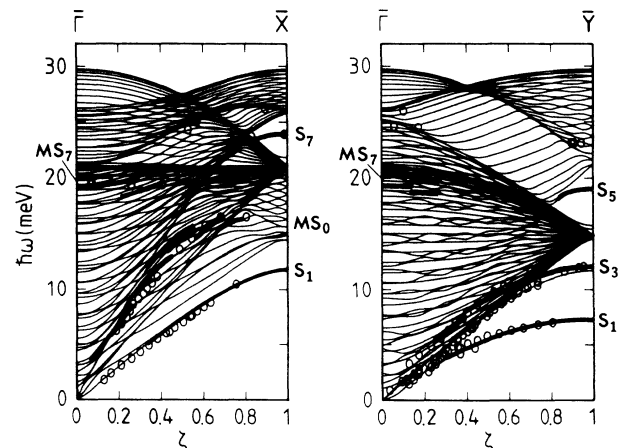


FIG. 9. Calculated phonon-dispersion curves along $\bar{\Gamma}\bar{X}$ and $\bar{\Gamma}\bar{Y}$ as in Fig. 7, but with modified force constants in the surface region (Tables I and II).

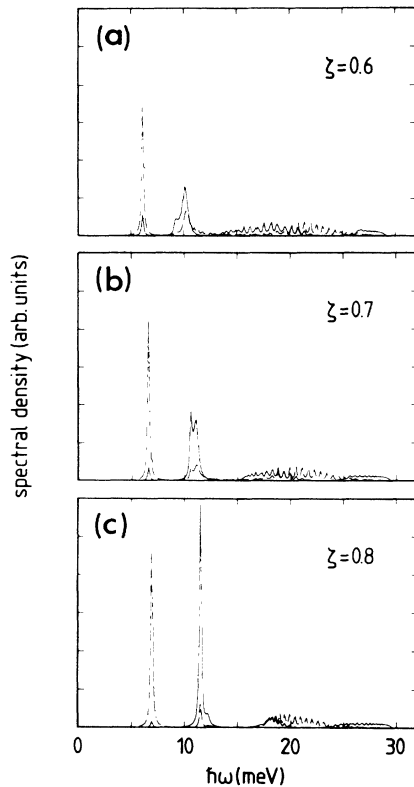


FIG. 10. Spectral density of states for three different reduced wave vectors ζ along $\bar{\Gamma}\bar{Y}$. Only sagittally polarized modes are shown; the dashed line corresponding to longitudinal polarization, the full line to transverse (z) polarization. The calculation was performed with the best fit force constants of Tables I and II, using a 60-layer-thick (110) slab crystal.

bulk-band edge E , while the mode at 10.2 meV corresponds to the surface resonance S_3 . In Fig. 10(c), $\zeta=0.8$, the order is reversed, the transverse bulk-band edge now being attributed to the higher energy shoulder of the doublet. In a simple picture both modes, E and S_3 , should intersect at $\zeta\sim 0.7$. However, as is evident from Fig. 10(b), this intersection is avoided, the modes hybridize (note the equal peak heights), and a splitting occurs. It should be pointed out that an avoided crossing is also known to occur between the MS_7 and MS_0 modes along the $\bar{\Gamma}\bar{X}$ direction;^{17,22} a similar hybridization of phonon modes has also been observed for physisorbed rare-gas layers on Pt(111) due to the avoided crossing of the adlayer mode and the substrate Rayleigh wave.³⁵ The spectral densities shown in Fig. 10 clearly illustrate the mech-

anism of the avoided crossing of the S_3 resonance and the transverse bulk-band edge. Further note that the vibrational amplitude of the edge mode rapidly declines beyond the avoided crossing; this amplitude is taken over by the resonance mode, which transforms into a true surface mode for ($\zeta > 0.7$) and which is totally z polarized at the \bar{Y} point. We believe that this result plausibly explains the fact that we observe three sagittally polarized acoustical modes for $\zeta < 0.8$, but only two such modes at the \bar{Y} point. An alternative explanation suggested in Ref. 18 for Pd(110), assuming three distinct modes, hardly accounts for the drastic decrease of the surface vibrational amplitude of the highest energy mode. In addition our calculation never showed the slightest indication of a significant peak above the bulk edge in the spectral density of the sagittally polarized modes for $\zeta > 0.8$. Actually, the experimental data in Ref. 18 like ours do not give any indication for such an additional surface phonon above $\zeta \geq 0.8$ and can be readily described within our model. This is also true for the Cu(110) data of Mason *et al.*¹⁵ In fact, we believe that the corresponding calculation of Black *et al.*²⁶ is consistent with our result: The calculated momentum-projected density of states exhibits the same features as shown in Fig. 10 and only yields two sagittally polarized modes for $\zeta > 0.8$.

Last but not least, it should be mentioned that Lehwald *et al.*¹⁴ were the first to stress the important contribution of the transverse bulk-band edge to the surface vibrational amplitude in this context. The limited resolution of HREELS did not allow for a direct experimental evidence, but their calculation of the relevant scattering cross sections clearly demonstrates this contribution.

To conclude, we believe that the scattering from the transverse bulk-band edge and the avoided crossing with the S_3 resonance mode can explain all experimental data reported so far on the acoustical modes along the $\bar{\Gamma}\bar{Y}$ direction for a series of (110) metal surfaces. The remaining question on the actual number of the modes observed has now received a fortunate answer: There are two classical surface modes, the Rayleigh wave (S_1) and a resonance (S_3); in addition there is scattering from the transverse bulk-band edge (E) which acquires surface-mode character through the hybridization with the S_3 surface resonance.

ACKNOWLEDGMENTS

We gratefully acknowledge Sieghart Lehwald, Francis Wolf, and Matthias Wuttig for clarifying discussions and for their help with setting up the slab-calculation computer program.

¹G. Benedek, in *Nonequilibrium Phonon Dynamics*, edited by W. E. Bron (Plenum, New York, 1985).

²R. E. Allen, G. P. Alldredge, and F. W. de Wette, *Phys. Rev. B* **4**, 1648 (1971).

³G. Brusdeylins, R. B. Doak, and J. P. Toennies, *Phys. Rev. Lett.* **46**, 437 (1981).

⁴J. P. Toennies, *Phys. Scr. T* **19**, 39 (1987).

⁵H. Ibach, *J. Vac. Sci. Technol. A* **5**, 419 (1987).

⁶J. P. Toennies, *J. Vac. Sci. Technol. A* **5**, 440 (1987).

⁷U. Harten, J. P. Toennies, and Ch. Wöll, *Faraday Discuss. Chem. Soc.* **80**, 137 (1985).

⁸U. Harten, J. P. Toennies, Ch. Wöll, and G. Zhang, *Phys. Rev. Lett.* **55**, 2308 (1985); K. Kern, R. David, R. L. Palmer, G. Comsa, and T. S. Rahman, *Phys. Rev. B* **33**, 4334 (1986).

- ⁹M. H. Mohamed, L. L. Kesmodel, B. M. Hall, and D. L. Mills, *Phys. Rev. B* **37**, 2763 (1988).
- ¹⁰S. Lehwald, J. M. Szeftel, H. Ibach, T. S. Rahman, and D. L. Mills, *Phys. Rev. Lett.* **50**, 518 (1983); M. Wuttig, R. Franchy, and H. Ibach, *Solid State Commun.* **57**, 445 (1986).
- ¹¹M. Wuttig, R. Franchy, and H. Ibach, *Z. Phys. B* **65**, 71 (1986).
- ¹²F. Jona and P. M. Marcus, in *The Structure of Surfaces II*, edited by J. F. van der Veen and M. A. van Hove (Springer, Berlin, 1988), p. 90.
- ¹³J. E. Inglesfield, *Prog. Surf. Sci.* **20**, 105 (1985).
- ¹⁴S. Lehwald, F. Wolf, H. Ibach, B. M. Hall, and D. L. Mills, *Surf. Sci.* **192**, 131 (1987).
- ¹⁵B. F. Mason, K. McGreer, and B. R. Williams, *Surf. Sci.* **130**, 282 (1983).
- ¹⁶J. P. Toennies and Ch. Wöll, *Phys. Rev. B* **36**, 4475 (1987).
- ¹⁷G. Bracco, R. Tatarek, F. Tommasini, U. Linke, and M. Persson, *Phys. Rev. B* **36**, 2928 (1987).
- ¹⁸A. M. Lahee, J. P. Toennies, and Ch. Wöll, *Surf. Sci.* **191**, 529 (1987).
- ¹⁹R. David, K. Kern, P. Zeppenfeld, and G. Comsa, *Rev. Sci. Instrum.* **57**, 2771 (1986).
- ²⁰L. K. Verheij and P. Zeppenfeld, *Rev. Sci. Instrum.* **58**, 2138 (1987).
- ²¹J. A. Stroschio, M. Persson, S. R. Bare, and W. Ho, *Phys. Rev. Lett.* **54**, 1428 (1984).
- ²²M. Persson, J. A. Stroschio, and W. Ho, *Phys. Scr.* **36**, 548 (1987).
- ²³V. Bortolani, A. Franchini, F. Nizzoli, and G. Santoro, *Phys. Rev. Lett.* **52**, 429 (1983).
- ²⁴K. M. Ho and K. P. Bohnen, *Phys. Rev. Lett.* **56**, 934 (1986).
- ²⁵A. G. Eguluz, A. A. Maradudin, and R. F. Wallis, *Phys. Rev. Lett.* **60**, 309 (1988).
- ²⁶J. E. Black, A. Franchini, V. Bortolani, G. Santoro, and R. F. Wallis, *Phys. Rev. B* **36**, 2996 (1987).
- ²⁷P. H. Dederichs, H. Schober, and D. J. Sellmyer, in *Landolt-Börnstein, Numerical Data and Functional Relationships in Science and Technology*, edited by K. H. Hellwege and J. L. Olsen (Springer, Berlin, 1981), Vol. 13a.
- ²⁸J. E. Black, F. C. Shanes, and R. F. Wallis, *Surf. Sci.* **133**, 199 (1983).
- ²⁹M. Copel, T. Gustafsson, W. R. Graham, and S. M. Yalisove, *Phys. Rev. B* **33**, 8110 (1986).
- ³⁰R. M. Badger, *J. Chem. Phys.* **2**, 128 (1934); **3**, 710 (1935); *Phys. Rev.* **48**, 284 (1935).
- ³¹A. P. Baddorf, I. W. Lyo, E. W. Plummer, and H. L. Davis, *J. Vac. Sci. Technol. A* **5**, 782 (1987).
- ³²A. P. Baddorf, Ph.D. thesis, University of Pennsylvania, 1987.
- ³³K. H. Rieder and W. Stocker, *Surf. Sci.* **164**, 55 (1985); K. Christmann, V. Penka, R. J. Behm, F. Chenab, and G. Ertl, *Solid State Commun.* **51**, 487 (1984); V. Penka, K. Christmann, and G. Ertl, *Surf. Sci.* **136**, 307 (1984).
- ³⁴M. Bader, A. Puschmann, C. Ocal, and J. Haase, *Phys. Rev. Lett.* **57**, 3273 (1986); H. Niehus and G. Comsa, *Surf. Sci.* **140**, 18 (1984).
- ³⁵K. Kern, P. Zeppenfeld, R. David, and G. Comsa, *Phys. Rev. B* **35**, 886 (1987).

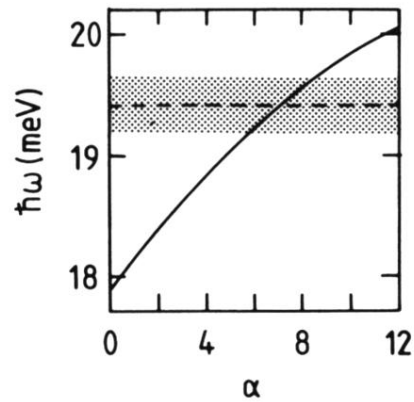


FIG. 8. Vibrational energy of the MS_7 resonance at the $\bar{\Gamma}$ point as a function of α [Eq. (2)], as obtained from the spectral density of states calculated with the force constants ϕ''_{12} , ϕ''_{13} , ϕ''_{23} , and ϕ''_{24} modified according to Eq. (2). The experimentally determined lattice relaxation Δd_{12} and Δd_{23} was used to calculate r_{ij} in Eq. (2). The measured energy $\hbar\omega_7 = 19.4 \pm 0.24$ meV, also shown in the figure, is best reproduced for $\alpha \approx 8$.